RESPONSE AND FAILURE OF METAL TANKS FROM IMPULSIVE SPOT LOADING: EXPERIMENTS AND CALCULATIONS

LEONARD E. SCHWER

APTEK, Inc., 4320 Stevens Creek Blvd., Suite 195, San Jose, CA 95129, U.S.A.

and

BAYARD S. HOLMES and STEVEN W. KIRKPATRICK

SRI International, 333 Ravenswood Ave., Menlo Park, CA 94025, U.S.A.

Abstract—A series of experiments were performed to determine the impulse intensity of a spot load that would cause failure in pressurized and unpressurized thin aluminum tanks. Strain histories in the vicinity of the failure were successfully recorded in several of the experiments. Finite element analyses of four experiments were performed to determine the details of the strain histories at the failure locations. Verification of the finite element modeling techniques are provided in a detailed comparison of strain histories for one of the experiments. A simple failure criterion, based on observations from the experimental and computational responses and additional biaxial tension tests, is used to predict the failure of the tanks.

1. INTRODUCTION

Thin metal shells are common structural elements used in shipping containers and in the structures of aircraft and road and rail vehicles. For many applications, it is necessary to predict the response of these structures under severe loading conditions that result in large deformations and ultimately material failure. The problem addressed in this paper is the prediction of the response up to and including rupture of pressurized and unpressurized thin aluminum shells subject to impulsive loading over a small area. In the experiments reported here an explosive technique was used to produce the loading, but the methods used could also be applied to other problems. This study was confined to right circular cylindrical shells made from aluminum alloy and loaded with circular spot loads with a pulse duration shorter than the response time of the structure. The loaded area was circular with a diameter equal to one-quarter of the shell diameter located at midheight on the shell as shown in Fig. 1. Because we were interested in loads resulting in shell rupture, the response in these experiments was characterized by large deformations and strains of the order of 10%. Both pressurized and unpressurized shells were tested.

Past analyses of the large deformation response of thin shells and plates have used both analytical and numerical methods. In general, the analytical solutions have been hampered by the complex kinematics of the response and have therefore been confined to very small displacements or to very specific problems. A key step in applying analytical methods is often an *a priori* knowledge of the kinematics of response, either through
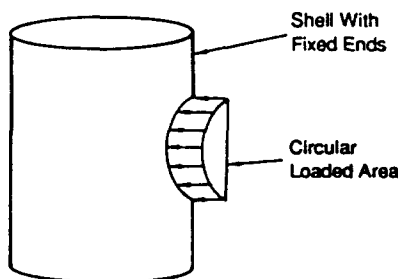

Fig. 1. Schematic of experiment.

observation or intuition. For example, Taylor (1942) proposed solutions for the response of plates to explosions by assuming a simplified constitutive model and compared the plate deformed shape to that of a soap film. Many more solutions of this type are available in the literature and are too numerous to list here. An extensive list of articles giving analytic solutions to problems of this type can be found in Jones (1985).

Numerical methods offer the advantage that geometric and material non-linearities can be treated explicitly. Recently developed shell elements for finite element code formulations allow treatment of shells at several levels of detail. The calculations shown here were performed with the Belytschko–Lin–Tsay formulation (Belytschko et al., 1984), as implemented by Hallquist and Benson (1986) into the DYNA3D finite element code. Previous results obtained with the Hughes–Liu formulation for shell elements (Hughes and Liu, 1981) were essentially identical, although the Belytschko–Lin–Tsay shell is less computationally demanding. The primary difference between these formulations as currently implemented is in their treatment of transverse shear terms in the shell. The Hughes–Liu formulation is based on a degenerated brick element and thus includes finite transverse shear terms. The Belytschko–Lin–Tsay formulation is based on Mindlin plate theory and therefore treats only infinitesimal transverse shear terms. Both these finite element formulations have been previously used to solve dynamic buckling response problems for thin shells similar to those treated here (Prantil et al., 1986; Kirkpatrick and Holmes, 1988). Because we did not find any differences between solutions obtained with these two elements as implemented in DYNA3D, computation time was the selection criterion.

We wanted to predict the response of thin aluminum shells including large deformations and fracture. To accomplish this, we used a limited number of experiments and finite element computations to investigate the response modes of the shells. The computations were compared to displacement and strain data taken from the experiments. A failure criterion for the shells was derived from static biaxial tension experiments and used to predict the critical load for shell rupture based on the strain history predicted by the finite element calculations. The predicted critical loads were compared with experimental data.

2. EXPERIMENTS

The shells used in the experiments were made from 0.635 mm thick 6061-T6 aluminum sheet, rolled into cylinders with a 30.48 cm o.d. and a 30.48 cm unsupported length. The resultant axial seam in the cylinder was butt welded with a lapped backing strip of aluminum for added strength. The ends of the cylinder were welded to heavy aluminum end rings that were designed to minimize stress concentrations. The end rings were anchored to a steel support frame.

The impulsive load was generated by mild detonating fuze (MDF) explosive. When detonated, MDF produced a fine spray of lead particles that produce a short duration load by impact (Lindberg and Murray, 1983). To obtain a spot load, a metal shield with a circular hole was used to intercept particles outside the loaded area, as shown in Fig. 2. The load produced by the lead spray has a duration of about 50 μs. An additional load is produced by the explosive products of the MDF and represents about 20% of the total load; this load has a duration of about 200 μs. The load distribution is nearly uniform over
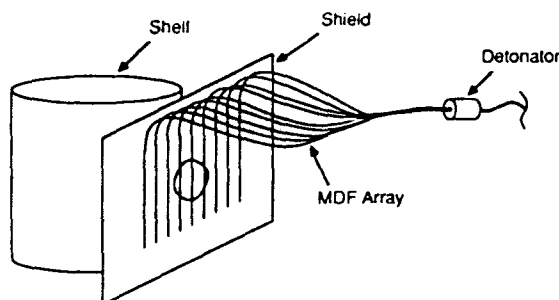

Fig. 2. Mild detonating fuze arrangement for experiments.

Table 1. Shell experiments

Experiment number	Pressure (MPa)	Impulse (Pa s)	Post-test condition
61	0.0	350	Indentation
31	0.0	440	Fracture
77	0.76	250	Outward bulge
33	0.76	250	Threshold fracture
78	0.76	285	Outward bulge
63	0.76	350	Burst

the loaded area with a sharp cut off at the edges. In any single experiment, the impulse intensity was known to within ±10%.

Instrumentation in the experiments consisted of high speed movies, strain gages and surface marks from which final shell elongations could be measured. Movies were taken of the inside of the shell with a framing rate of 10,000 frames s^{-1}. This data can be used to obtain the timing of events to within the time between frames (100 μs). Eight strain gages were used in those experiments with gages, giving strain histories at specific locations. The surface markings used to measure elongations consisted of pairs of indentations, about 0.02 mm diameter and spaced 1.516 cm apart. The pairs of indentations are called "Dracula" marks.

Six experiments are used here for comparison with analysis although more experiments were performed. In each of the experiments described here, the loaded area was 7.62 cm in diameter. The impulse intensity varied between 250 and 440 Pa s. Two tank shell internal pressures were used: zero gage pressure and 0.76 MPa. The latter pressure results in a hoop stress in the tank wall of two-thirds the yield stress of the aluminum. Table 1 lists the experiments.

In the unpressurized shells, the response consisted of a large elongated indentation with large axial tensile strains but small hoop strains due to the cylindrical geometry. Failure was through a single fracture in the hoop direction beginning at the center of the loaded spot. The first two experiments listed in Table 1 were unpressurized and were tested at 350 and 440 Pa s, respectively. Figure 3 shows the post-test front and side views of two unpressurized shells. Figure 3(a) shows the deformations of the shell tested at 350 Pa s in Experiment 61; the dark circular region at the center of the shell is the area that was directly exposed to the MDF and corresponds to the impulsively loaded region. The shell remained intact with no visual signs of cracking or tearing. Post-test deformations in the shell tested at the higher load level, Experiment 31, are shown in Fig. 3(b). A fracture oriented in the hoop direction occurred at the midheight of the shell and propagated to the ends of the deformed region.

Response in the pressurized shells was quite different from that observed in the unpressurized shells. The high speed movies showed that the early time response was similar, producing a conical indentation in the shell. However, the amount of indentation for a given load was reduced and was immediately followed by an outward rebound of the shell. The indented area snapped through resulting in a bulge about the size of the loaded area. Examination of the strain gage records showed that large tensile axial strains occurred first on the inward motion, followed by smaller compressive axial strains during the initial phase of the rebound motion. Finally, large tensile hoop strains occurred during the last part of the outward motion. Failure occurs when fractures, oriented in the axial direction near the center of the spot load, develop during the outward portion of the response. At sufficiently high load levels, the fractures are driven by the internal pressure and the shells fail catastrophically by bursting open.

Figure 4 shows the shells from two experiments. Figure 4(a) shows the bulge that occurred in Shell 33 tested at 250 Pa s. In this experiment, a small axial crack occurred at the center of the loaded spot as shown in the closeup of the shell in Fig. 4(b). Figure 4(c) shows the post-test condition of Shell 63, tested at 350 Pa s causing the shell to burst. In this experiment, an axial fracture originated at the center of the loaded region and propagated to

the ends of the shell where it bifurcated and propagated along the end rings. The two other pressurized shell experiments, listed in Table 1 as Experiments 77 and 78, were added because post-test examination of Shell 33 indicated that the lead spray may have produced surface damage to the material within the loaded region. This surface damage may have precipitated the small crack that occurred in this experiment. Based on the added experiments, we concluded that the critical load for the pressurized shells was between 285 and 350 Pa s.

3. FINITE ELEMENT ANALYSIS

The purpose of the finite element analysis is to provide detailed information about the stress and strain response of the shell structures. This response can then be used with theoretical or empirical failure models to predict critical load levels for failure. In this section we describe the finite element modeling and validation of the model by comparing the predicted strain response with the measurements obtained in pressurized shell Experiment 77. Analyses of three other experiments, at higher impulse levels with and without internal pressure, were also performed. These latter experiments were not instrumented with strain gages but results based on the calculations are presented for subsequent comparison with observed and predicted failure modes. We also compare calculated and measured strain histories for Experiment 77 to demonstrate that the complex strain history leading to failure can be calculated accurately. Experiment 77 was a test of a pressurized shell in which fracture did not occur.

3.1. Finite element modeling

The analyses were performed using the Lawrence Livermore National Laboratory finite element code DYNA3D (Hallquist and Benson, 1986). DYNA3D is a non-linear transient Lagrangian finite element code with explicit temporal integration. The computational grid comprising 669 nodes with 69 brick and 522 shell elements is shown in Fig. 5; only one quarter of the full grid was used because the simulation has two planes of symmetry. Typical CPU times for a 1.5 ms simulation with this grid configuration are 5.5 h on a MicroVAX II. The relatively coarse grid (compared with those used in the analysis of flood loaded tanks (Kirkpatrick and Holmes, 1988)) was chosen because short wavelength pulse buckling† and edge effects from the end rings were not considered to be important parts of the structural response. An even coarser grid model, our initial model, produced similar results to those presented in this section.

The heavy aluminum end rings which affect the end closures of the cylinder and provide an inertial constraint on the shell motion were explicitly included in the model. The 1 in. thick (2.54 cm) by 2 in. long (5.08 cm) end rings are modeled with solid 8 node brick elements, as can be seen at the end of the shell model shown in Fig. 5. The shell element portion of the grid was continued over the end rings and the shell elements were merged with the outer surface of the brick elements to provide continuity of the shell-to-brick interface for the shell element rotational degrees of freedom. The butt welded axial seam, used to form a cylinder, was not included in the model, because its effect on the shell response under the spot load was not considered to be important.

The constitutive model used for the 6061-T6 aluminum consists of a linear elastic portion, with a modulus of 69,000 MPa (10^7 psi), a Von Mises yield criterion with a yield stress of 275 MPa (40,000 psi), a hardening modulus of 586 MPa (85,000 psi), and kinematic hardening. Figure 6 compares this bilinear model with the results of tensile tests of the shell material.

The preload from the internal pressure in the tank is modeled by prescribing a uniform pressure on all of the elements comprising the cylindrical surface. Nodal forces in the axial direction are applied at the end of the shell to produce an axial preload stress which is half of the circumferential preload stress. These pressures and forces are prescribed to be

---

†When pulse buckling is an important part of the response, the initial imperfections in the shell need to be included in the calculation. Kirkpatrick and Holmes (1988) include a detailed characterization of the imperfections typical of this type of shell construction and their effects on computed shell response.
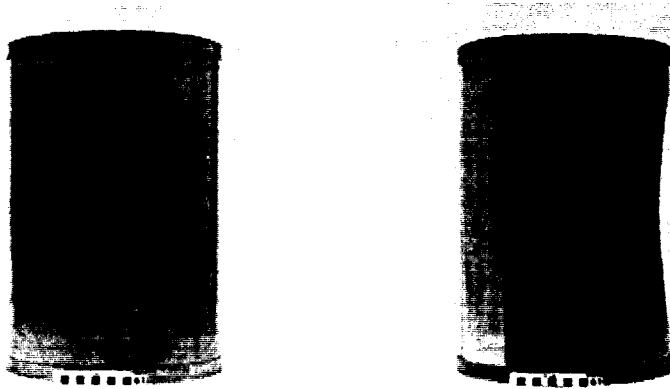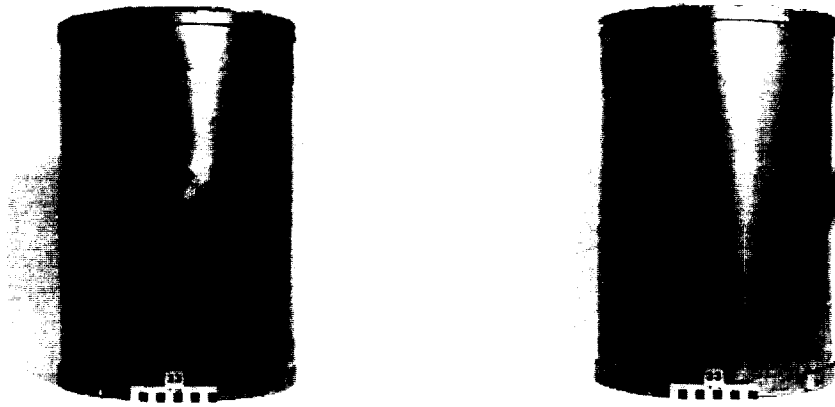
(a) Front and Side View of Shell 61
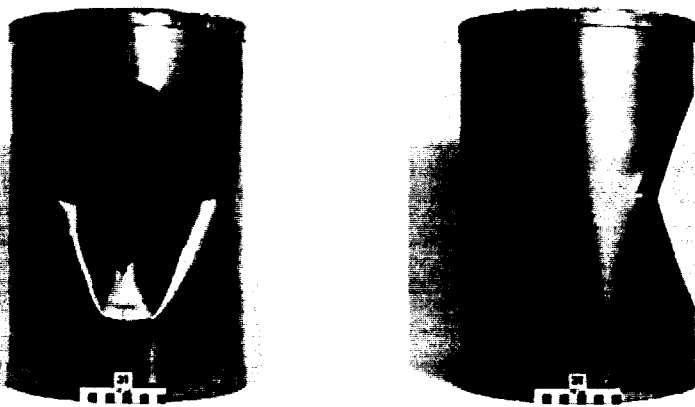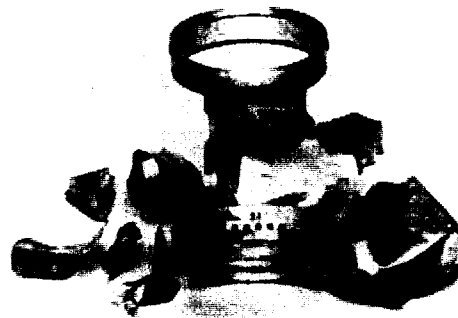

(b) Front and Side View of Shell 31

Fig. 3. Response of unpressurized shells.
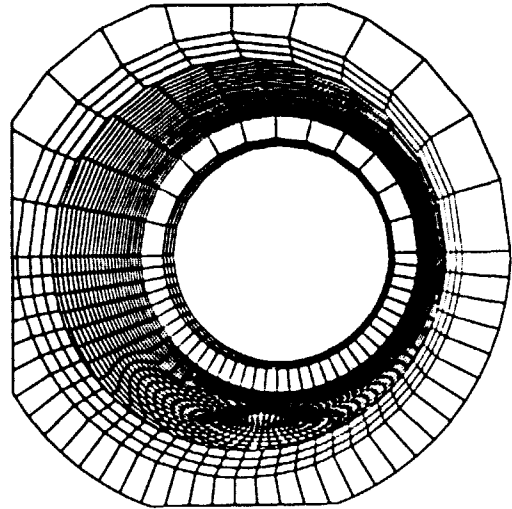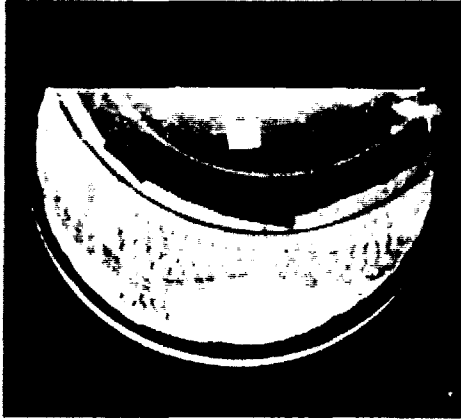
(a) Front and Side View of Shell 33

(b) Closeup of Shell 33

(c) Response of Shell 63

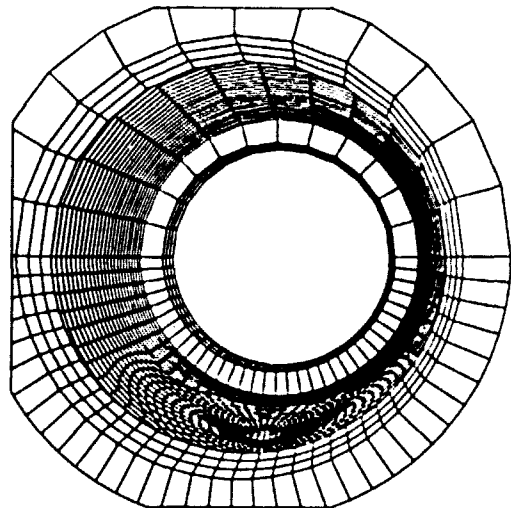Fig. 4. Response of pressurized shells.

Time = 0.12 ms

Time = 0.58 ms

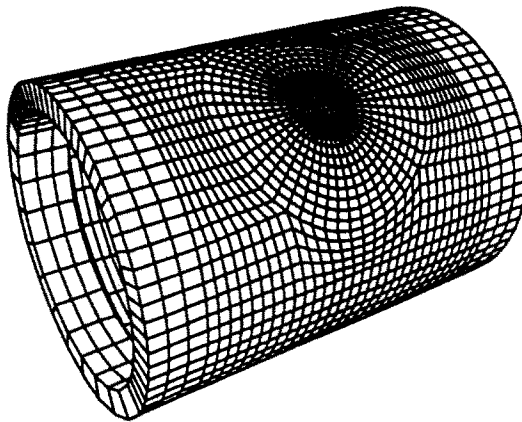Fig. 9. Maximum inward and outward deformed shapes.

Fig. 5. Computational grid.

constant during the calculation, which neglects the effects of shocks or rarefactions in the internal gas used to pressurize the experiments; simple calculations indicated that these effects could increase the internal pressure by 20% under the loaded area. The preload equilibrium stress state is computed by using the dynamic relaxation option in DYNA3D prior to applying the impulsive loading; computation of the preload accounts for approximately 60% of the total CPU time.

The impulsive spot load, produced by the lead spray, is applied to the computational grid as an initial uniform velocity over the loaded area; the initial velocity is related to the impulse intensity through the relation $I = \rho h V_0$, where ρ is the density and h the thickness of the shell. The spot loaded area corresponds to the interior of the innermost uniform circle of elements shown in Fig. 5. The initial velocity was applied normal to a plane that is tangent to the center of the spot; the velocity vectors do not curve around the circumference of the shell. The magnitudes of the velocity vectors at the nodes along the spot edge were reduced to account for the added lumped mass at these nodes from elements outside the spot; the total momentum of the spot load is properly prescribed.

The additional load produced by the detonation products from the mild detonating fuze is modeled here as a pressure history (in addition to the constant internal pressure) applied to the elements under the spot load. The effect of the blast pressure outside the area loaded by the lead spray is thought to be small and was neglected. This late-time pressure
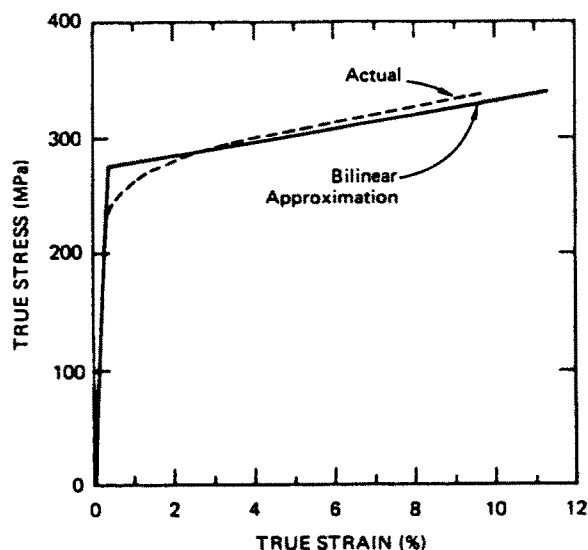
Fig. 6. Measured stress–strain curve for simple tension and its bilinear approximation.
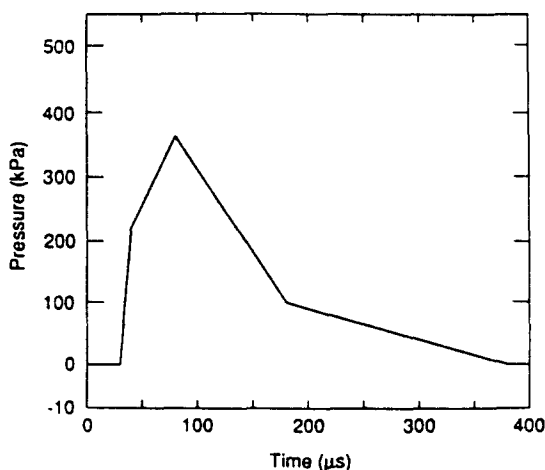
Fig. 7. External pressure history used in calculations to simulate additional blast loading.

pulse was measured in one of the experiments and an approximation of this pulse, used in the calculation of Experiment 77, is shown in Fig. 7.

3.2. *Structural response*

Before discussing the comparison of the calculated and measured strains for the pressurized shell of Experiment 77, we present an overview of the structural response using only the calculated results. Figure 8 shows the calculated radial displacement history at the center of the spot load. The initial radial movement of the shell is directed inward towards the axis of the cylinder. As the initial kinetic energy imparted to the shell is converted into strain energy during deformation and work against the internal pressure, the inward velocity is reduced. At approximately 0.12 ms, the maximum inward displacement is reached, and the internal pressure begins to push the spot center radially outward. As will be shown subsequently, the initially outward rebound motion produces an elastic unloading followed by compressive axial stresses and a partial reversal of the axial strains. As the loaded spot is driven outward beyond its original position, tensile hoop stresses and strains are produced. At approximately 0.59 ms the center of the loaded spot reaches a maximum outward displacement where it oscillates elastically. The deformation of the tank as viewed from the tank end is shown in Fig. 9 at the times corresponding to maximum inward and outward radial deflections; both the observed and calculated shapes are shown. The deformed region in the figure is only slightly larger than the spot size.
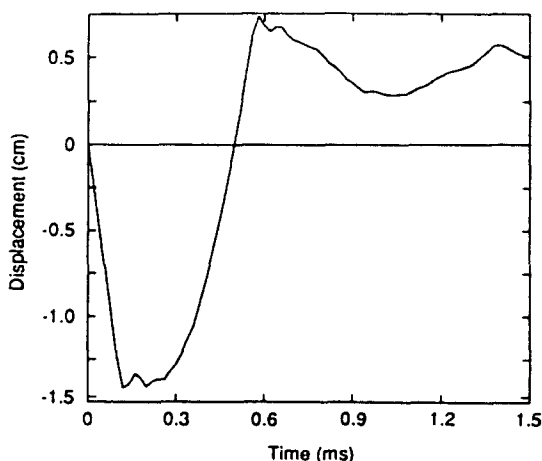

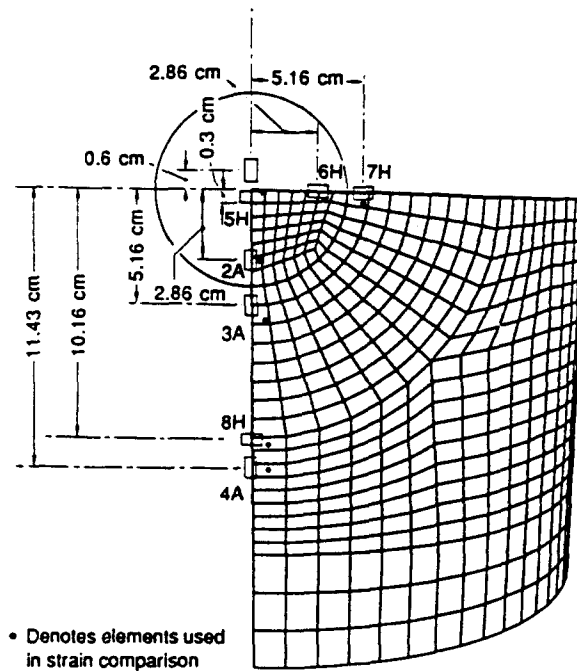Fig. 8. Radial displacement at spot center calculated for Experiment 77.

Fig. 10. Strain gage locations

Figure 10 shows the location of the strain gages in the experiment and their positions relative to the computational grid and spot loaded region (indicated by the full circle in Fig. 10). There are four gages measuring strains along the shell axis, 1A, 2A, 3A and 4A, at 0°, and four gages, 5H 8H, to measure hoop strains. Three of the hoop gages, 5H, 6H and 7H, are located near or on the mid-plane. The fourth hoop gage, 8H, is located at 0° about half way between the spot center and the end support. These eight inner surface strain gage locations will be referenced in the comparisons between computed and experimental strains.

Figure 11(a) shows the computed axial strain histories at all four axial gage locations. The strain history near the center of the spot load, gage 1A, had the largest axial strain, which rose to a peak of 4.2% at 0.12 ms. The strain remains nearly constant until 0.4 ms, and then starts to decrease. This time corresponds to the beginning of the outward motion of the loaded area as indicated by the reversal in the radial displacement history shown in Fig. 8.

Figure 11(b) shows the computed hoop strain histories at all four hoop gage locations. Again, the location near the center of the loaded spot, gage 5H, has the largest strain. The history of the maximum hoop strain response is the complement of the axial strain response. The hoop strain is small during the inward motion of the spot, but rapidly increases as the spot rebounds and moves outward beyond its original radial position. The hoop strain is small during the inward motion of the shell because circumferential line elements "snap through" and change their curvature in an almost inextensible manner; a small amount of compressive strain is shown in Fig. 11(b) at the start of the strain record and again at 0.4 ms as the material under the spot begins to expand beyond its initial radial position.

Thus, the strain response of a pressurized spot-loaded tank is dominated by axial straining during the initial inward deformation and by hoop straining on the subsequent outward deformation. This characteristic of the response is important when considering tank failure. If the critical failure strain of the material is not exceeded during the initial inward motion, no circumferential cracks or tears are formed, but the subsequent outward motion may exceed the critical strain and produce axial cracks or tears. Later we will use a failure criterion based on the history of axial and hoop strains to anticipate fracture.
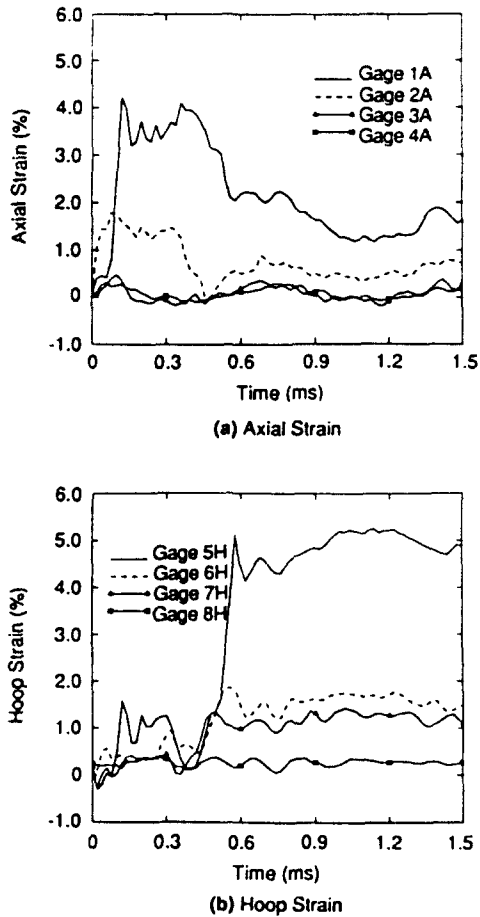
(a) Axial Strain

(b) Hoop Strain

Fig. 11. Calculated strain histories for Experiment 77.

3.3. Comparison with experimental data

Figure 12 shows a comparison of the experimental (solid line) and calculated (dashed line) axial strain records at the four axial gage locations. The initial static axial and hoop strains from the internal pressure have been calculated and added to the experimental strain records. The addition of the preload strains to the experimental data is necessary because the strain gages are zeroed after the tank has been pressurized.

In general, the calculated strains agree well with the measured strains. The greatest discrepancy is at gage 1A (Fig. 12(a)), where the maximum calculated strain, 4.25%, is greater than the measured strain and the measured strain decreases rapidly after reaching a peak value of 2.7%. Post-test inspection of this gage showed that it had delaminated from the shell during the test and probably did not measure the peak strain at the gage location.

Figure 13 shows a comparison of the experimental and calculated hoop strain records at the four hoop gage locations. Strain gage 5H, located near the center of the spot load, failed very early in the test and is not included in the comparison. In general, the calculated strains agree qualitatively with the experimental strains, but the magnitude of the calculated hoop strain at gage 7H is larger than the experimental value by a factor of 1.4. Also, the calculated strains indicate that the strain reversal associated with the outward motion of the spot loaded region begins about 0.2 ms earlier than observed in the experiment (Figs 13(b)–(d)).

Several factors may contribute to the observed differences between the analysis and the experiments. In calculations made before the additional pressure pulse from the detonation products was incorporated into the model, the discrepancies in strain magnitude and rebound timing were larger. The effect of this late time pressure is to reduce the magnitude of the hoop strain during the outward motion and delay the onset of the outward motion.
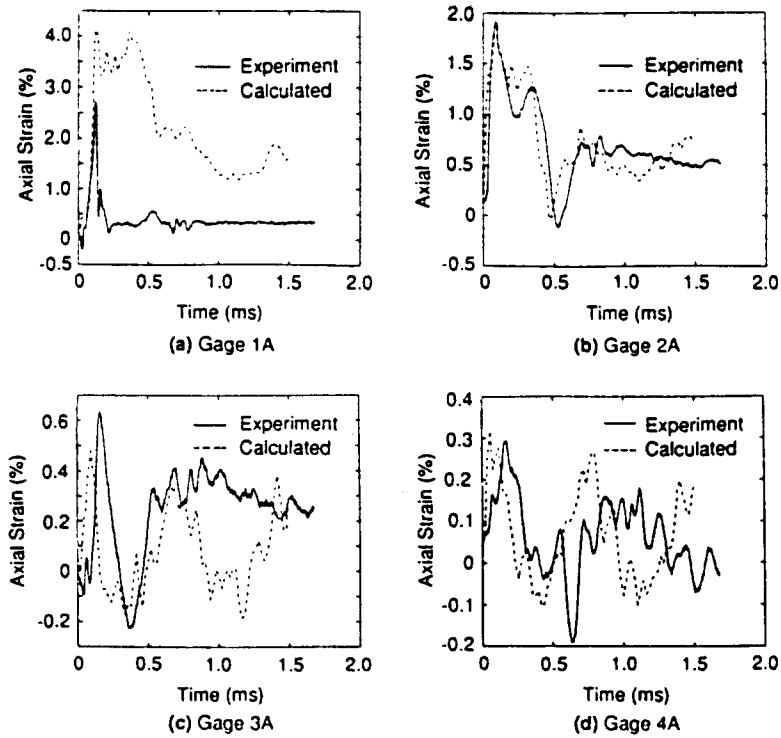
Fig. 12. Comparison of measured and computed axial strain histories for Experiment 77.

Thus it appears that the structural response may be sensitive to the history of this load. We also ignored the influence of pressure waves in the gas inside the shell. As the shell moves rapidly inward, the effective pressure under the spot could increase by as much as 20%, based on simple model calculations, and the subsequent rarefaction waves could reduce the effective pressure by 5%. The effect of these pressure changes is still under investigation.
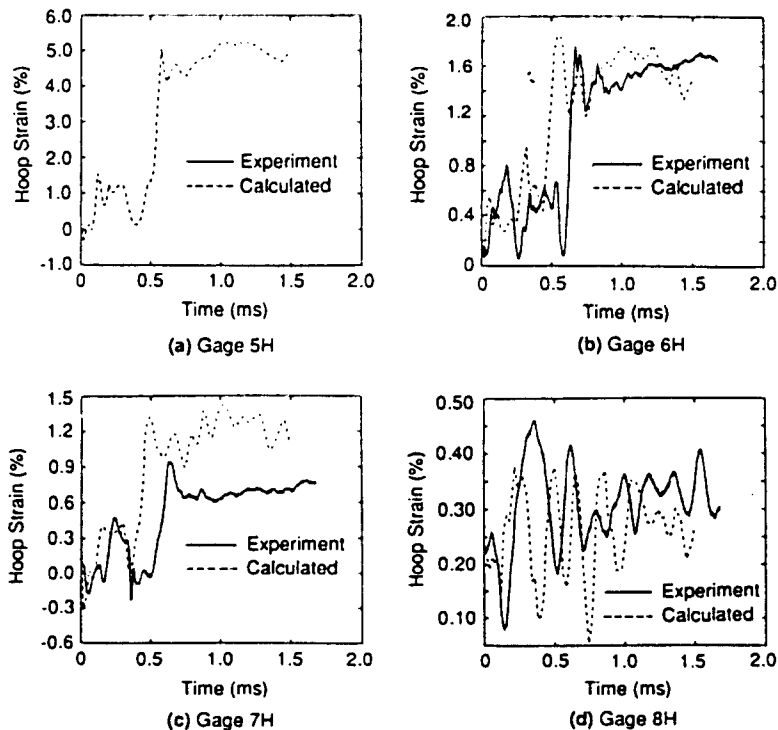

Fig. 13. Comparison of measured and computed hoop strain histories for Experiment 77.

Table 2. Calculated maximum tensile strains in percent

Experiment number	Strain gage location								Failure
	1A	2A	3A	4A	5H	6H	7H	8H	
61	8.5	6.5	3.5	1.0	2.5	0.8	0.4	0.1	None
31	12.5	8.5	4.7	1.2	4.5	1.0	0.4	0.2	Hoop crack
33/37	4.0	1.9	0.6	0.3	5.0	1.7	1.2	0.3	Crack/none
63	8.0	3.6	1.3	0.3	10.5	4.6	1.9	0.5	Burst

3.4. *Analysis of three other experiments*

Calculations similar to those described above were performed for Experiments 63, 61, and 31. Since these experiments were not instrumented with strain gages, a direct comparison between calculated and measured response cannot be made. However, using the results of the calculations, we can make the following observations about the strain response.

(1) Experiment 63 was similar to Experiments 33 and 77, but the impulse intensity was increased to 350 Pa s. As would be expected, the higher load level produces more strain, roughly by a factor of 2, in both the axial and hoop directions, and also lengthens the duration of the inward motion of the spot-loaded region by about 0.2 ms. Shell 63 burst during the experiment.

(2) Experiment 61 had the same impulse level as Experiment 63, but the tank was unpressurized. The calculated strain records for these two cases were very similar during the inward motion. The effect of internal pressure is only apparent at later times when the spot-loaded region of the pressurized tank moves outward. In an unpressurized tank no outward motion of the spot-loaded region occurs and the shell is permanently deformed inward.

(3) Experiment 31 was similar to Experiment 61, but the impulse was increased to 440 Pa s. Again, as expected, the higher load level produces more strain, by a factor of 1.5 in the axial direction and 2.0 in the hoop direction. The maximum axial strain predicted in this experiment was 12.5%. The shell used in Experiment 31 fractured circumferentially during the experiment.

3.5. *Correlation of observed damage and calculated strains*

Table 2 lists the maximum calculated tensile strains for the four experiments analyzed. The right-most column lists the failure mode, if any, observed during or after the experiments. Comparisons of the maximum tensile strain with the experimental results lead to the following observations.

(1) The unpressurized shell experiments, Experiments 61 and 31, indicate that failure in these shells occurs at axial tensile strains between 8.5 and 12.5%. Significant hoop tensile strains were also predicted at the center of the loaded spot for these experiments, of 2.5 and 4.5%, respectively. However, the magnitude of the hoop strains decreases rapidly with distance from the spot center.

(2) The pressurized shell experiments indicate that fracture occurs after a complex sequence of loading consisting of axial tension followed by compression and finally large hoop tensile strains. The maximum tensile hoop strain at which an axial fracture occurred was between 5 and 10.5%, based on a comparison of predicted strains for Experiments 77 and 63.

4. PREDICTING FAILURE

Examination of the shells after the experiments showed that failure occurred through a necking localization that ran circumferentially in the unpressurized shells and axially in
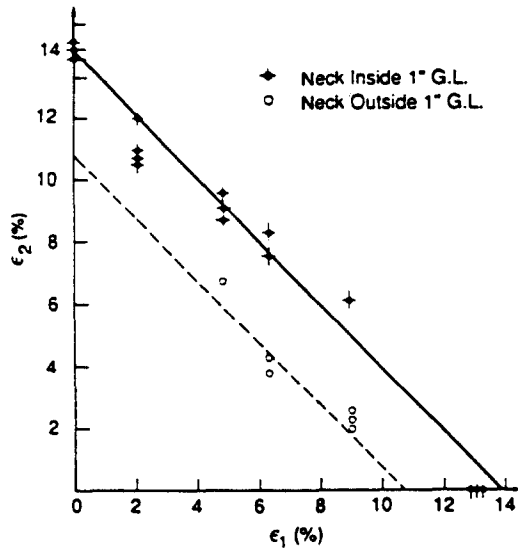
Fig. 14. Strains at failure for biaxial tension tests with sequential loading: Step 1, ε_1 across rolling direction; Step 2, ε_2 along rolling direction.

the pressured shells. The tensile strains at which failure occurred were different for the two cases. Based on comparison of the calculations with the results of the experiments, the tensile strains in unpressurized shells, Experiments 61 and 31, reached 8.5 and 12.5% before failure. Fracture and busting in the pressurized shells, Experiments 33 and 63, occurred after a complex strain history, but final tensile hoop strains at failure were between 5 and 10.5%. It was not possible to better define the final tensile strains in the shells from the data obtained in the experiments.

The failure of these thin shells is similar to the failures that occur during metal forming operations such as the stamping of sheet metal parts. Much recent work has focused on the formability limits of metal sheets. Experiments and analyses of the necking failure of sheets have shown that the liming strains are strongly dependent on the loading path (Needleman and Tvergaard, 1984; Prantil et al., 1986). In particular, experiments with proportional biaxial straining have shown an increase in strain to failure over uniaxial experiments. Because we did not have data for the particular loading path observed in the current experiments (a sequential biaxial loading) we carried out experiments to directly model this loading path.

A series of static tensile experiments were performed on the shell material to measure its stress–strain behavior and examine the effect of load history on failure. Large tensile coupons of the shell material, 15 × 5 cm gage dimensions, were first pulled perpendicular to the rolling direction (the shell axial direction) to strains of approximately 2, 4, 6, and 9%. Tensile coupons were then cut from these specimens along the rolling direction (the shell hoop direction) and these were then pulled to failure; this approximates the sequential loading of the pressurized shells at the spot center, without the intermediate axial compressive strains. Strains in both tensile tests were measured with an extensometer.

The resultant pairs of axial and hoop (across and along the rolling direction) strains measured at failure in these tensile tests are plotted in Fig. 14. Note that the two sets of data given in the figure correspond to coupons that failed within the measured gage length (solid marks) of the extensometer and those that failed outside the gage length (open circles).† The separation between the two sets of data, about 3% strain, represents the elongation that occurs in the necked region of the tensile coupon as it fails. The data plotted

†The strain to failure (solid marks) depends on the gage length used to measure the strain; the smaller the gage length the larger the failure strain. Hence the dashed curve (open circles) where localization begins should be used as a threshold to indicate failure in an analysis.
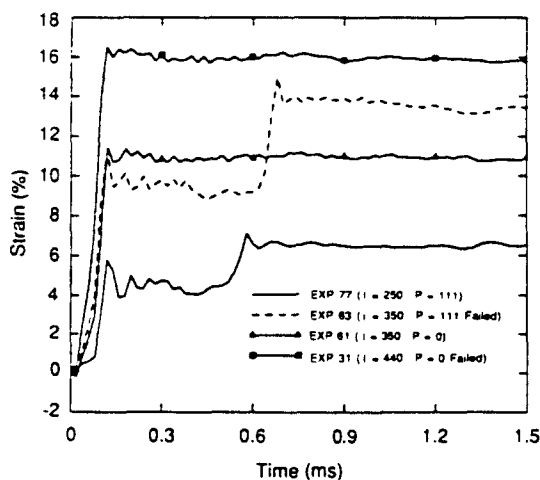
Fig. 15. Sum of calculated principal strain histories at gage 1.

in Fig. 14 suggest that the sum of the axial and hoop direction strains is nearly constant at failure. In addition, localization and failure occur when the sum of the uniform strains in the two directions reaches approximately 11 and 14%. This is not a general failure criterion and may only be applicable for the specific loading path in our experiments. In fact, it would be an extremely poor failure criterion for some proportional loading paths (Needleman and Tvergaard, 1984; Chin-Chan, 1982), but it is not inconsistent with more general solutions to the necking problem. We have examined the onset of necking for loading histories in these tensile tests using the more general methods described in Lemonds and Curran (1987) and Rice (1976) and obtained results similar to those seen in the tensile tests. However, at this time these general failure criteria are not implemented into DYNA3D.

As a test of the failure criterion suggested by the biaxial tensile tests, we compared the algebraic sums of the principal strain histories calculated for the four experiments with the failure strains measured in the tensile tests. Figure 15 shows the sum of the principal strain histories calculated for each of the four experiments. These plots show sums in excess of 14% in the two experiments where failure occurred. In the two experiments where failure did not occur the sum of the two strains was less than 12%. Recognizing the difficulty in comparing the calculated strains, which do not include necking effects, and the observed failure in the experiments, we tentatively conclude that failure occurs when the sum of the principal strains reaches 12–14%. This is consistent with the results of the biaxial tensile tests where localization and failure occurred when the sum of the principle strains reached 11–14%.

5. CONCLUSIONS

A combination of experiments and analysis was undertaken to describe the entire response process of thin aluminum shells subject to spot loads up to and including failure. Very good comparisons were obtained between measured response and that predicted with the finite element code DYNA3D. These results suggest that detailed strain and displacement histories can be predicted for these shells. A simple failure criterion based on biaxial tension tests was used to predict failure. The failure criterion suggested by the tension tests was consistent with failure observed in the shell experiments, but it may not be general enough for use in other problems.

REFERENCES

Belytschko, T., Lin, J. I. and Tsay, C. (1984). Explicit algorithms for the dynamics of shells. *Comp. Meth. Appl. Mech. Engng* **42**, 225–251.

Chin-Chan, Chu (1982). An investigation of the strain path dependence of the formability limit curve. *Int. J. Solids Structures* **18**, 205–215.

Hallquist, J. O. and Benson, D. J. (1986). *DYN3D User's Manual (Nonlinear Dynamic Analysis of Structures in Three Dimensions)*. University of California, Lawrence Livermore National Laboratory, Report UCID-19592, Revision 2.

Hughes, T. J. R. and Liu, W. K. (1981). Nonlinear finite element analysis of shells: Part I. Three-dimensional shells. *Comp. Meth. Appl. Mech. Engng* **26**, 331–362.

Jones, N. (1985). Recent progress in the dynamic plastic behavior of structures: Part IV. *Shock Vibr. Dig.* **17**(2), 35–47; see also Parts I and II **10**(9), 21–23 (1978) and **10**, 13–19 (1978), and Part III **13**, 3–16 (1981).

Kirkpatrick, S. W. and Holmes, B. S. (1988). Structural response of thin cylindrical shells subjected to impulsive external loads. *AIAA J.* **26**(1), 96–103 (1988).

Lemonds, J. and Curran, D. (1987). Analysis of strain localization in 6061-T6 aluminum sheets. Tech. Rept., SRI International, Menlo Park, California.

Lindberg, H. E. and Murray, Y. M. (1983). Calibration and analysis of the SPLAT (Spray Lead at Target) impulse simulation technique. SRI International Report, Menlo Park, California.

Needleman, A. and Tvergaard, V. (1984). Limits to formability in rate sensitive metal sheets. In *Mechanical Behavior of Materials IV* (Edited by J. Carlson and N. G. Ohlson). Pergamon Press, Oxford.

Prantil, V. C., Kirkpatrick, S., Holmes, B. S. and Hallquist, J. O. (1986). Response of a very thin shell under an impulsive radial load. In *Finite Element Methods for Plate and Shell Structures: Vol. 2: Formulations and Algorithms* (Edited by T. J. R. Hughes and E. Hinton), pp. 252–262. Pineridge Press, Swansea, U.K.

Rice, J. R. (1976). The localization of plastic deformations. In *Theoretical and Applied Mechanics* (Edited by W. T. Koiter), pp. 207–220. North-Holland, Amsterdam.

Taylor, G. I. (1942). The distortion under pressure of a diaphragm which is clamped along its edge and stressed beyond the elastic limit. In *The Scientific Papers of Sir Geofrey Ingram Taylor*, pp. 496–502. Cambridge University Press, Cambridge.